Electronic Supplementary Information

Photoanodes for water oxidation with visible light based on a pentacyclic quinoid organic dye enabling proton-coupled electron transfer

Giulia Alice Volpato,[a‖] Martina Marasi, [a,b‖] Thomas Gobbato, [a] Francesca Valentini, [b] Federica Sabuzi,[b] Valeria Gagliardi,[a,b] Alessandro Bonetto,[c] Antonio Marcomini,[c] Serena Berardi,*[d] Valeria Conte,[b] Marcella Bonchio,[a] Stefano Caramori,[d] Pierluca Galloni*[b] and Andrea Sartorel*[a]

a Department of Chemical Sciences, University of Padova, via Marzolo 1 35131 Padova (Italy). andrea.sartorel@unipd.it

b Department of Chemical Science and Technologies , University of Rome "Tor Vergata" via della Ricerca Scientifica, snc 00133 Roma, Italy. galloni@scienze.uniroma2.it

c Dept. Environmental Sciences, Informatics and Statistics, University Ca' Foscari Venice, Vegapark, Via delle Industrie 21/8, 30175 Marghera, Venice, Italy.

d Department of Chemical and Pharmaceutical Sciences, University of Ferrara, and Centro Interuniversitario per la Conversione Chimica dell'Energia Solare (SolarChem), sez. di Ferrara, Via L. Borsari 46, 44121 Ferrara, Italy. brrsrn@unife.it

‖ These authors equally contributed.

SUMMARY

1. Equipment

UV-Vis absorption spectra were performed on Perkin-Elmer Lambda 45, Varian Cary 100 and Varian Cary 50 spectrophotometers. Quartz cuvettes with 1 mm optical path were used for UV-Vis absorption spectra of solutions, at a temperature of 25°C.

Measurements of pH were done with a Metrohm pH-meter.

Quantitative determination of Ru_4POM was performed with a PerkinElmer Nexion 350 ICP-MS.

(Photo)Electrochemical measurements were performed using an AMEL potentiostat-galvanostat model 7050 or a BAS EC Epsilon potentiostat-galvanostat, in a 3 electrodes configuration. Illumination was provided by a LOT-Quantum Design solar simulator AM 1.5 G, equipped with a 400 nm cut-off filter to exclude the contribution of SnO_2. The measurements of Incident Photon-to-Current Efficiency were performed by irradiation with a 175 W Xenon lamp coupled to an Applied Photophysics monochromator with a 380 nm cut off filter.

Transient absorption spectroscopy (TAS) experiments were performed with a previously described apparatus,[1] using the 532 nm harmonic of a nanosecond Nd:YAG laser (Continuum Surelite II) and a monochromatic probe beam from a pulsed Xe lamp.

AFM analyses. The photoelectrodes topology was characterized with an Agilent 5500 SPM, equipped with a scanner AFM multipurpose (scanning range 90 µm x 90 µm x 7 µm). The AFM images were analysed with the WSxM 5.0 software. The analyses were performed within a departmental service at DiSC provided by Dr. Andrea Basagni.

SEM-EDX analyses. SEM was performed with a Zeiss Sigma HD microscope, equipped with a Schottky FEG source, one detector for backscattered electrons and two detectors for secondary electrons (InLens and Everhart Thornley). The microscope is coupled to an EDX detector (from Oxford Instruments, x-act PentaFET Precision) for X-rays microanalysis, working in energy dispersive mode. EDX data were acquired and analysed through the AZtec Nanoanalysis software from Oxford Instruments. The analyses were performed within a departmental service at DiSC provided by Dr. Andrea Basagni.

2. Methods

2.1. Synthesis

Synthesis of 1-(3-ethoxycarbonylpropyl)KuQuinone.[2] 1-(3-ethoxycarbonylpropyl)KuQuinone has been synthesized according to a previously reported literature procedure. [2] 1 g (5.75 mmol) of 2-hydroxy-1,4-naphthoquinone, 2.5 g (8 mmol) of anhydrous Cs_2CO_3 and 62 mg (0.33 mmol) of sublimated ferrocene were dissolved in 22 ml of DMSO (kept overnight over anhydrous K_2CO_3 prior to use). Afterwards, 12 mmol of ethyl 6-bromohexanoate were added and the mixture was kept under stirring at 114°C for 41 hours. Then, it was diluted with 100 ml of dichloromethane and filtered. The filtrate was washed with brine (2× 500 ml), dried over anhydrous Na_2SO_4 and filtered. Solvent was removed under reduced pressure and the obtained brown powder was purified by *plug* chromatography (SiO_2, eluent CH_2Cl_2). The isolated purple powder (173 mg, 0.40 mmol, 14% yield) was precipitated from dichloromethane-hexane and then washed with pentane. ^{1}H NMR in $CDCl_3$: δ 18.20 (s, 1H), δ 8.27-8.22 (m, 4H), δ 7.79-7.71 (m, 4H), δ 4.15-4.11 (q, 2H), δ 3.53-3.50 (t, 2H), δ 2.50-2.47 (t, 2H), δ 2.09-2.04 (m, 2H), δ 1.25-1.23 (t, 3H). HRMS (ESI^-) *m/z*: $[M-H]^-$ calcd for $C_{27}H_{20}O_6$ 439.1187; found 439.1207.

Synthesis of 1-(3-carboxylpropyl)KuQuinone (KuQ(O)$_3$OH).[2] $KuQ(O)_3OH$ was obtained by hydrolysis of the corresponding ester: 45 mg of 1-(3-ethoxycarbonylpropyl)KuQuinone (0.10 mmol) were dissolved in 50 ml of THF. Afterwards, 5 ml of a saturated solution of NaOH in MeOH were added and the system was kept under stirring overnight and checked by TLC (SiO_2, eluent CH_2Cl_2). After neutralization with 0.1 M HCl, a purple precipitate was obtained. 39.2 mg of the product have been obtained as a purple powder (0.095 mmol, 95% yield). HRMS (ESI^-) *m/z*: $[M-H]^-$ calcd. for $C_{25}H_{16}O_6$ 411.0874; found 411.0898. UV−vis in THF [λ_{max}, nm (ε, $M^{-1}cm^{-1}$)]: 563 (15250); 529 (13400); 370 (6800).

2.2. Preparation of SnO_2|$KuQ(O)_3OH$|Ru_4POM photoanodes

The SnO_2 colloidal paste was prepared by addition of 2.1 mL of glacial acetic acid to 50 mL of commercial colloidal SnO_2 (dimension of nanoparticles ca. 60 nm; 30% w/w): the solution was vigorously stirred for 2 hours and then put in oven inside an autoclave at 220°C for 12 hours. After cooling to room temperature, 3.5 g of copolymer polyetylenglicole bisphenol A epicloridin (Carbowax ®) were added, and the resulting paste was stirred for 6 hours. [3]

10 x 10 cm FTO (Fluorine Tin Oxide) conducting glass was cleaned by 10 minutes sonication in Alconox and 10 minutes sonication in 2-propanol. The SnO_2 colloidal paste was then deposited on the FTO substrate by doctor blading and sintered in oven with the following temperature ramp: 30 mins → 25 - 70 °C; 40 mins → 70 °C; 30 mins → 70 - 450 °C; 20 mins → 450 °C; 10 mins → 450 - 500 °C; 30 mins → 500 °C. [4]

After cutting to the desired dimension, the FTO|SnO_2 electrodes were sensitized by 20-hour soaking in a 0.13 mM solution of $KuQ(O)_3OH$ dye in tetrahydrofurane (THF), followed by rinsing with THF. The electrodes were then pre-treated by immersion in acidic solution (pH < 3), to obtain the neutral acidic form of KuQ, $KuQ(O)_3OH$, by re-protonation of the enolate formed during the soaking procedure. The loading of $KuQ(O)_3OH$ dye onto the electrodes was estimated from the difference in absorption of the solution before and after soaking.

To prepare the SnO_2|$KuQ(O)_3OH$|Ru_4POM photoanodes, the sensitized SnO_2|$KuQ(O)_3OH$ photoanodes were soaked for 30 minutes in a 4 mM Ru_4POM solution in milliQ water, containing 1% m/v of Nafion (from 10% m/m Nafion suspension in water): the electrodes were then slowly removed from the solution to avoid the accumulation of drops at the bottom of the electrode, let to dry for 10 minutes, and then rinsed by immersion in milliQ water. SnO_2|Nafion and SnO_2|$KuQ(O)_3OH$|Nafion control samples were prepared by 30-minutes soaking in a 1% Nafion solution in milliQ water, followed by 10 minutes drying and rinsing. SnO_2|Ru_4POM-Nafion control samples were prepared with the same procedure of SnO_2|$KuQ(O)_3OH$|Ru_4POM photoanodes.

2.3. Preparation of ZrO_2 film for TAS experiments

ZrO_2 colloidal paste was prepared according to a previously reported procedure,[4] then doctor-bladed onto FTO slides and annealed at 550°C for 30 minutes.

2.4. Transient absorption spectroscopy (TAS)

TAS experiments were performed using the 532 nm harmonic of a nanosecond Nd:YAG laser (Continuum Surelite II) and a monochromatic probe beam from a pulsed Xe lamp. Transient measurements on thin films were obtained by orienting the electrodes at an angle of approximately 45° with respect to the excitation, with a laser fluence of ca. 5 mJ/cm^2/pulse. The probe light transmitted by the sample was passed through a stack of two 532 nm notch filters to eliminate the scattered laser and then focused into a 50 lines/mm grating before reaching the photomultiplier, biased at 500 V. The differential absorbance (ΔOD) traces on the ns/μs timescale were recorded with an oscilloscope input impedance of either 50 or 350 Ω. The 350 Ω impedance was preferentially used to amplify the transient signals from the sensitized films, which were generally weaker than those recorded in solution, due to the non-optimal transparency of both SnO_2 and ZrO_2 films. The ΔOD traces were normally averaged over 30 shots to obtain an acceptable Signal-to-Noise (S/N) ratio and then fitted with multiexponential functions in order to obtain noise free traces to construct the difference TA spectra.

2.5. (Photo)electrochemistry. (Photo)electrochemical experiments were performed in a 3-electrode configuration using Pt as counter electrode and Ag/AgCl 3 M NaCl as reference electrode. Illumination was provided by a solar simulator (AM 1.5G light), positioned 20 cm far from the sample (1 sun intensity, irradiance = 100 mW/cm^2), equipped with a 400 nm cut-off filter.

Due to the high current registered, the LSVs in ascorbate sacrificial hole scavenger were performed with compensation (positive feedback iR compensation) of the ohmic drop caused by the resistance of the electrolyte (Rs = 50 Ω). [5]

- **38 mM Na_2SiF_6/60 mM $NaHCO_3$ buffer pH 5.8:** 0.705 g Na_2SiF_6 and 0.512 g of $NaHCO_3$ were added to 100 mL of milliQ water, and then stirred overnight to facilitate dissolution of Na_2SiF_6. If required, the pH was adjusted with Na_2SiF_6 or $NaHCO_3$ stock solutions.

- **Ascorbate-based electrolytic solution**: 1.98 g (0.01 mol) of sodium ascorbate $C_6H_7O_6Na$ were dissolved in 100 ml of milliQ water to obtain a 0.1 M solution (pH=8.39), and then acidified to pH 5.8 by addition of 200 µL of 0.5 M H_2SO_4.

2.6. Quantitative determination of Ru_4POM by ICP-MS. Each electrode was soaked in 3 mL of aqua regia in a separate Teflon vessel. After 1.5 hour, the remaining glass support was removed and washed 4 times with 1.25 ml of MilliQ water, and then 1 mL HF was added to the mixture. The vessels were than sealed and microwave-heated by means of a Milestone Ethos 1600, following a previously reported temperature ramp. The excess of HF was neutralized by addition of 2 mL of a H_3BO_4 solution, and microwave-heated again. Samples were than diluted to 30 mL in MilliQ water and analyzed by ICP-MS. The instrument was optimized in standard mode and Y^{89} and Re^{187} were chosen as internal standards. For the quantification of W and Ru, the masses 182 and 101 were selected, respectively, and a 9-points calibration curve was used for the mass estimation. The surface loading of Ru_4POM on the electrodes was then calculated upon normalization for the area of the SnO_2 deposit on each electrode.

2.7. Generator-collector method for O_2 detection

The FTO collectors were cleaned by 10 minutes sonication in KOH/iPrOH solution and then in iPrOH, followed by thermal treatment in oven at 500°C for 30 minutes. Cu tape contacts were applied to generator and collector electrodes. The photoanode under investigation was then sandwiched to an FTO collector using two unstretched Parafilm strips both as spacer (200 µm spacing) and insulator for preventing short-cut between the Cu contacts: the Parafilm strips were previously cut in a L-shape to minimize oxygen loss during the measurements, while still allowing the electrolyte access for capillary forces. The sandwich was pressed for 60 s at 60°C.

The optimal potential for O_2 reduction on FTO at pH 5.8 was estimated to be -0.9 V vs Ag/AgCl by CV in O_2-saturated Na_2SiF_6/$NaHCO_3$ buffer at pH 5.8. The generator-collector experiment was then performed employing a bipotentiostat to simultaneously control the potential applied at the two working electrodes, WE1 being the O_2 generator (photoanode) and WE2 being the O_2 collector (FTO electrode); Pt was used as counter electrode and Ag/AgCl 3M NaCl as reference electrode. The electrolytic solution was purged with N_2 before each measure.

The illumination was provided by a white LED lamp with a 400 nm cut-off filter, positioned 5 cm far from the back of the sandwiched photoanode (resulting irradiance = 25 mW cm^{-2} in the 400-600 nm range) to achieve an irradiance as close as possible to the one provided by the solar simulator positioned at 20 cm (resulting irradiance = 56 mW cm^{-2} in the 400-600 nm range). A comparison of emission spectra and irradiances (acquired with the Avantes AvaSpec-USB2 Fiber Optic Spectrometer) of the LED lamp and of the solar simulator, in both cases with 400 nm cut-off filter, is reported below.

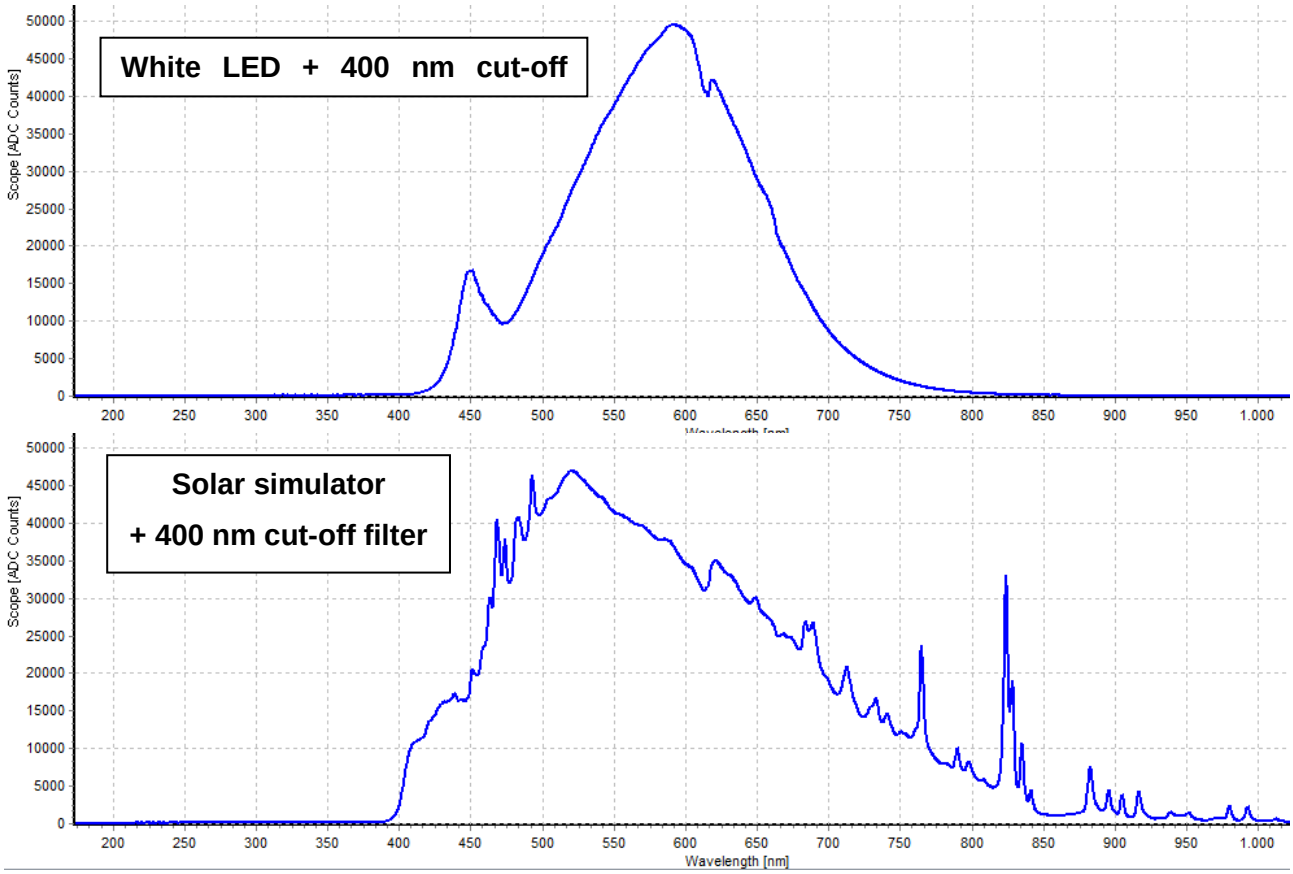

		Irradiance (mW/cm^2)		
Source	**Distance**	**Whole emission range**	**400 - 850 nm**	**400 - 600 nm**
White LED	5 cm	33	32	25
Solar Simulator (AM 1.5G)	20 cm	100	78	48

In a typical experiment, the generator was held at a constant potential of 0.6 V vs Ag/AgCl and the collector at -0.9 V vs Ag/AgCl: currents at both the working electrodes were recorded in the dark for 30-60 seconds, to eliminate any residual oxygen trace by reduction at the collector, then during 150 s of illumination, then in the dark for additional 100 s, to allow the diffusion of O_2 across the solution. The faradaic efficiency for O_2 production, η_{O2}, can be calculated with the following equation:

$$\eta_{O_2} = \frac{Q_{coll}}{Q_{gen}} \cdot \eta_{coll}$$

where Q_{coll} is the integrated current measured at the Collector electrode, Q_{gen} is the integrated photocurrent measured at the generator electrode, and η_{coll} is the collector efficiency (which must be quantified under the specific set-up and experimental conditions used).[6] In particular, the corresponding stable current values measured in the initial dark step were subtracted to the registered current values. The corrected current values were then integrated (to yield Q_{gen} and Q_{coll}) using the "subtract baseline" tool in Origin, in order to account also for the current registered in the final dark step of the experiments. As regards η_{coll}, it has been estimated to be 56%, from G-C experiments on FTO-FTO sandwiches [6] prepared in the same way of the analogous photoanode-FTO ones: different G-C experiments were performed by progressively increasing the potential applied at the FTO generator from 1.5 to 1.9 V vs Ag/AgCl (Figure S11); a calibration curve was derived from a plot of Q_{coll} vs Q_{gen} (Figure S11); the collection efficiency was then obtained as the slope of the linear fit of the curve.

2.8. IPCE and APCE measurements.

The photocurrents and photon flux were determined at different wavelengths by dark/light chronoamperometry steps, at 0.56 V vs SCE, in Na_2SiF_6/$NaHCO_3$ buffer solution, pH 5.8. Chronoamperometric experiments (30s light/dark intervals) were performed under monochromatic irradiation, in the range λ= 390 - 630 nm, with 10 nm steps, generated by a 175 W Xenon lamp coupled to an Applied Photophysics monochromator with a 380 nm cut off filter. The irradiance, i.e. the irradiated power per area, was calculated at each wavelength by a calibrated silicon photodiode. Incident Photon-to-Current Efficiency (IPCE) and Absorbed Photon-to-Current Efficiency (APCE) values were calculated according to the following equations:

$$IPCE(\%) = \frac{\Phi_{e^-}}{\Phi_{ph}} \cdot 100 = \frac{J_\lambda \cdot \frac{10^{-2}}{F}}{\frac{I_\lambda}{N_A} \cdot E_\lambda} \cdot 100 \approx 1240 \cdot \frac{J_\lambda}{\lambda \cdot I_\lambda}$$

$$APCE_\lambda = \frac{IPCE_\lambda}{LHE_\lambda} \qquad LHE_\lambda = 1 - 10^{-\Delta Abs(\lambda)}$$

where Φ_{e^-} and Φ_{ph} are the flux of electrons and incident photons (mol $s^{-1}m^{-2}$), respectively, J_λ is the steady state photocurrent density (μA cm^{-2}) at a certain value of λ, F is the Faraday's constant, I_λ is the irradiance, defined as the irradiated power at λ per unit area, N_A is Avogadro's number, E_λ = $hc/\lambda \cdot 10^{-9}$ is the energy (eV) of a photon of wavelength λ(nm), and LHE_λ is the Light Harvesting Efficiency, calculated from the UV-Vis absorption spectrum of the photoanode after subtraction of the SnO_2 substrate contribution.

3. Supplementary Figures and Tables

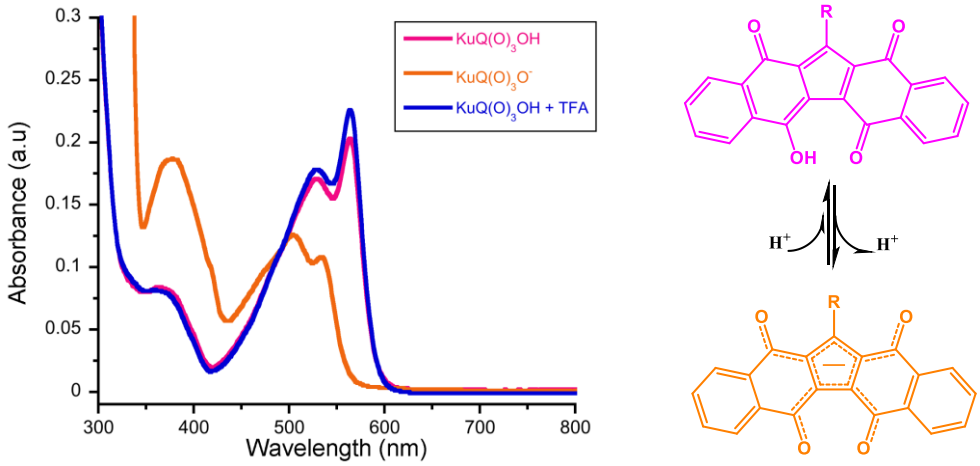

Figure S1. Absorption spectra of 0.015mM $KuQ(O)_3OH$ solution in THF (purple) and after addition of 2.5 mM NaOH solution (orange) and 2.5 mM TFA solution (blue); optical path: 10mm. Absorption maxima: $KuQ(O)_3OH$ + TFA: 563 nm (ε = 15000), 529 nm (ε = 11700); $KuQ(O)_3O^-$: 534 nm (ε =7200), 504 nm (ε =8400), 382 nm (ε =12400). Right: acid-base equilibrium between the acidic $KuQ(O)_3OH$ enol form (purple) and the basic $KuQ(O)_3O^-$ enolate form (orange).

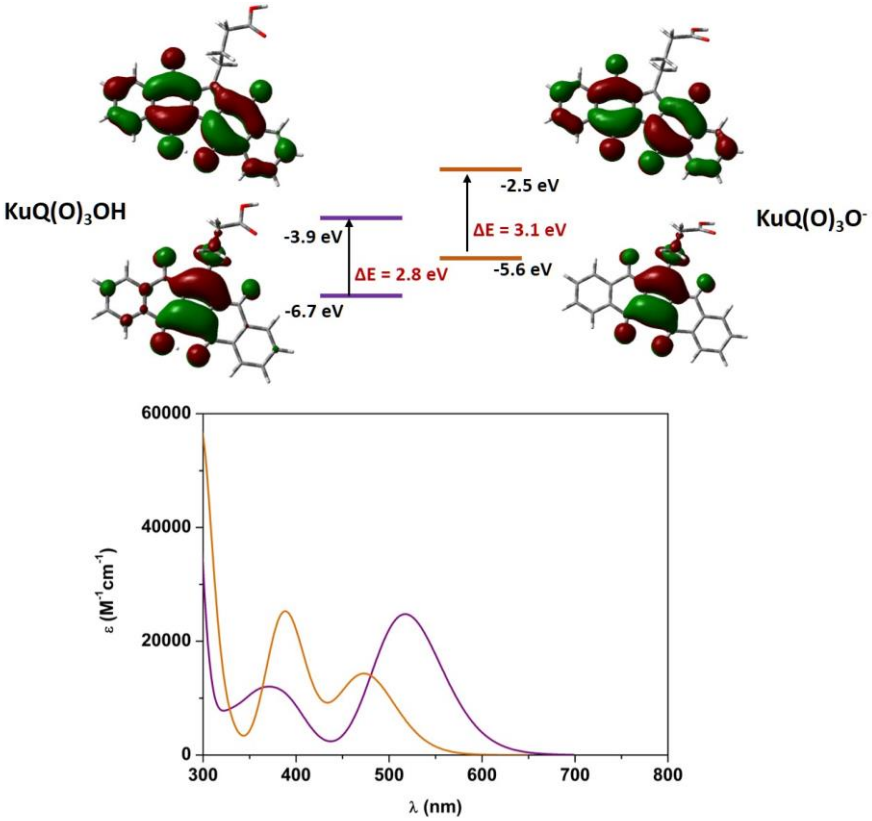

Figure S2. Top: HOMO and LUMO molecular orbitals distribution of $KuQ(O)_3OH$ (left) and $KuQ(O)_3O^-$ (right). Geometry optimization and orbital energies calculations performed with DFT B3LYP/6-31G+(d,p) level of theory, including a polarizable continuum model (PCM) of THF. Bottom: calculated absorption spectra of $KuQ(O)_3OH$ (purple line) and $KuQ(O)_3O^-$ (orange line). Absorption spectra calculated with TD-DFT B3LYP/6-31G+(d,p), including a polarizable continuum model of THF.

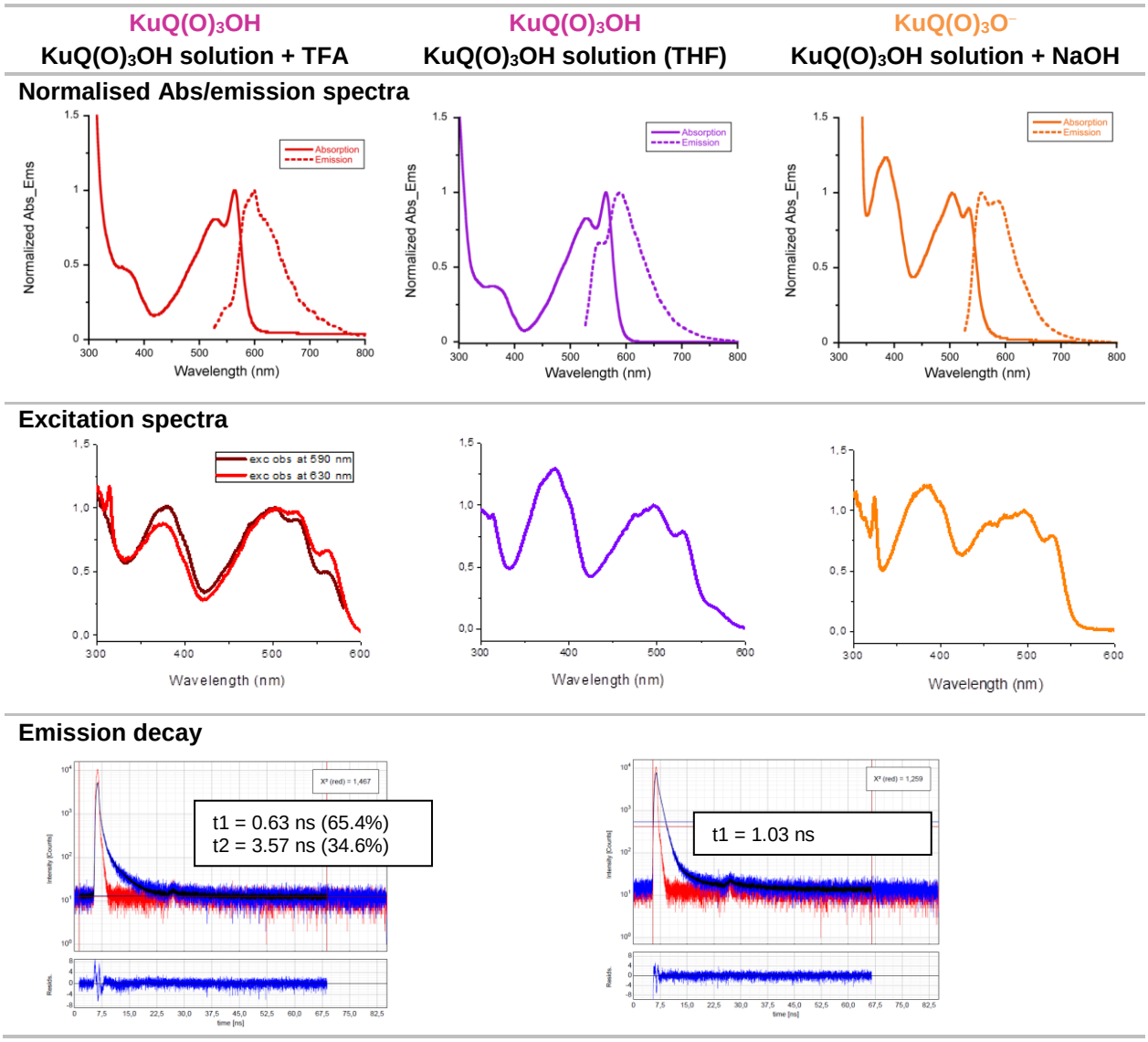

Figure S3. Normalised absorption and emission spectra (λexc= 480 nm, slit 5-5), Excitation spectra of $KuQ(O)_3OH$+TFA, $KuQ(O)_3OH$ and $KuQ(O)_3O^-$. Emission decay of $KuQ(O)_3OH$ in THF+TFA and in THF or in THF + NaOH and $KuQ(O)_3O^-$ (λexc= 480 nm, λem= 600 nm, slit 5-5). The fluorescence quantum yield in solution is (i) QY = 3.2% for $KuQ(O)_3OH$ 0.015 M in THF, (ii) QY = 1.1% for $KuQ(O)_3OH$ 0.015 M in THF + TFA, QY = 7.9% for $KuQ(O)_3OH$ 0.015 M in THF + NaOH, using a free-base octaethylporphyrin reference (QY = 0.16 in toluene, see V. S. Chirvony et al. J. Phys. Chem. B, 2000, 104, 9909), excitation at 510 nm.

The excitation spectra registered in THF and in THF + NaOH match with the absorption of $KuQ(O)_3O^-$, suggesting this as the main emitter under these conditions; in THF + TFA, the excitation spectrum matches the absorption of a mixture of $KuQ(O)_3OH$ and $KuQ(O)_3O^-$, thus being both emitting under these conditions. This scenario is further confirmed by emission decay analysis: while in THF and in THF + NaOH a monoexponential decay with a lifetime of 1.03 ns is observed, in THF+TFA a biexponential decay with lifetimes of 3.57 ns (34.6% contribution) and 0.63 ns (65.4% contribution) is observed, suggesting two emitting species. The shortening of the lifetime of the fast component observed in the presence of TFA (0.63 ns vs 1.03 ns) may be due solvent polarity effects or increase of non radiative quenching owing to hydrogen bonding between the dye and TFA.

The emission properties of the dye are influenced by the acidity of the enol in the ground and in the excited states. The E^{00} of $KuQ(O)_3OH$ (protonated enol) can thus be estimated by the crossing of the normalised absorption/emission in the presence of TFA; this results at 575 nm, corresponding to an E^{00} = 2.16 eV. The E^{00} of $KuQ(O)_3O^-$ (enolate) can be estimated from the crossing of normalised absorption/emission in the presence of NaOH; this results at 544 nm, corresponding to an E^{00} = 2.28 eV.

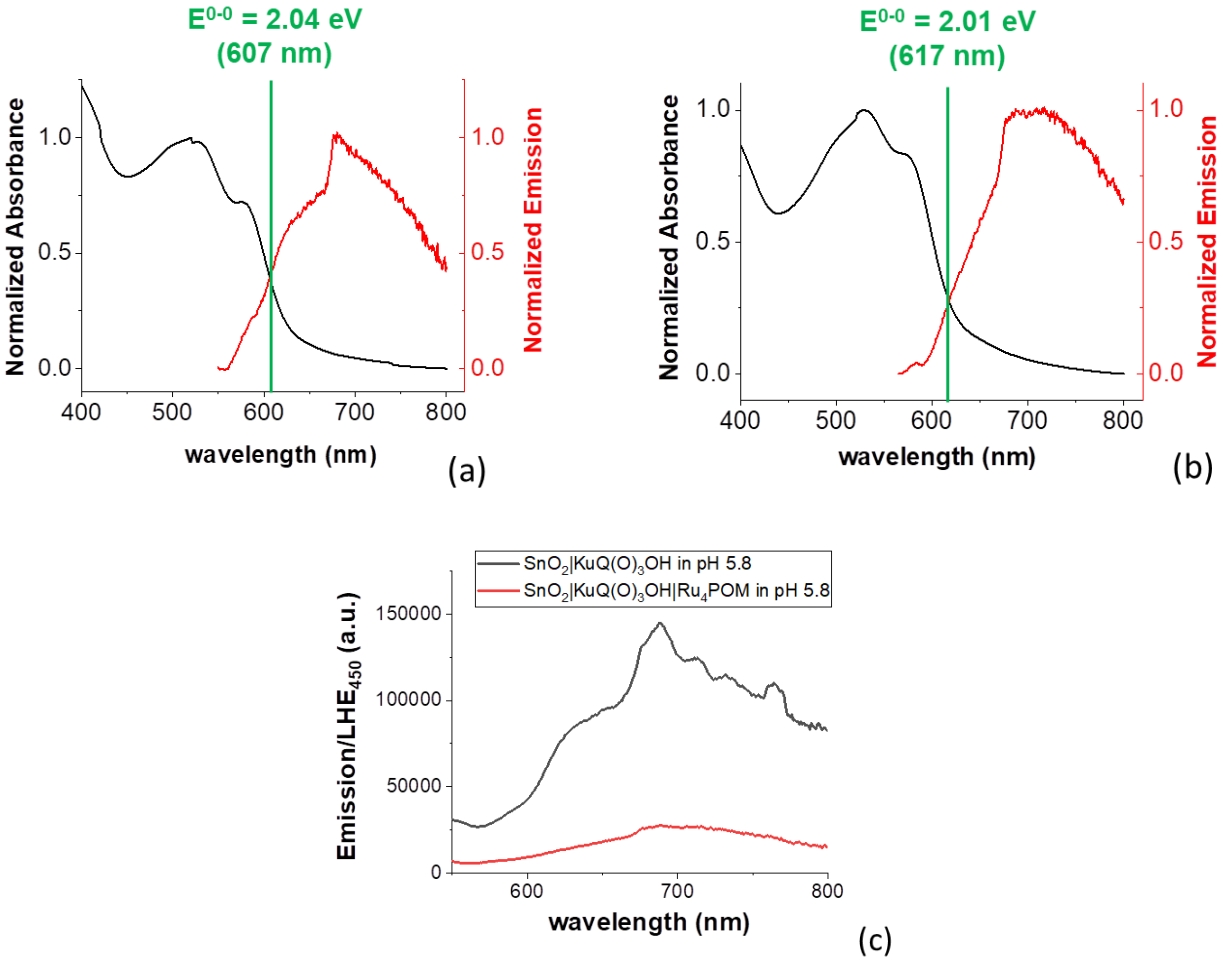

Figure S4. (a-b) Normalized absorption (black trace) and emission (red trace, λ_{exc} = 450 nm) spectra of SnO_2|KuQ(O)$_3$OH immersed in 0.1 M Na_2SiF_6/$NaHCO_3$ buffer pH 5.8 (a) and in H_2SO_4 pH 2 (b). The crossing points, corresponding to the $E^{0\text{-}0}$ values, are indicated in green. (c) Emission spectra of SnO_2|KuQ(O)$_3$OH (black trace) and SnO_2|KuQ(O)$_3$OH|Ru_4POM (red trace) normalized for the LHE at λ_{exc} = 450 nm. Both electrodes were immersed in 0.1 M Na_2SiF_6/$NaHCO_3$ buffer pH 5.8.

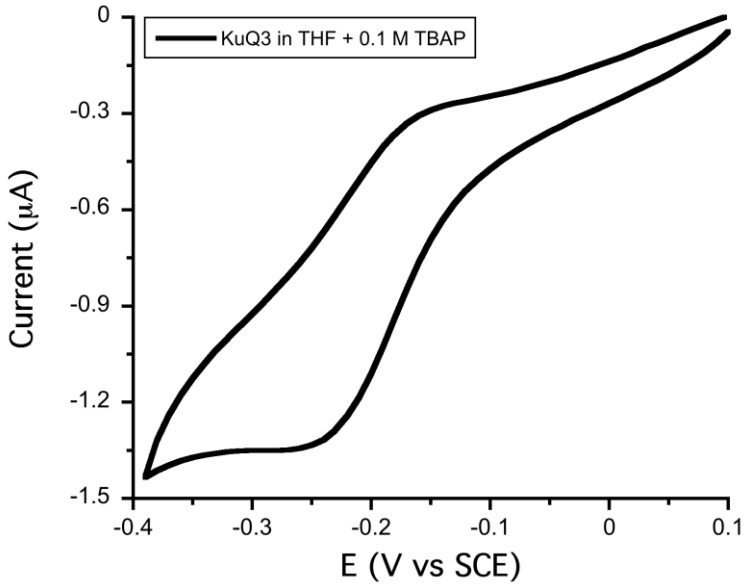

Figure S5. Cyclic voltammetry of 0.13 mM $KuQ(O)_3OH$ solution in THF with 0.1 TBAP as supporting electrolyte. WE = GC, CE = Pt, RE = Ag/AgCl 3M NaCl, scan rate = 100 mV/s.

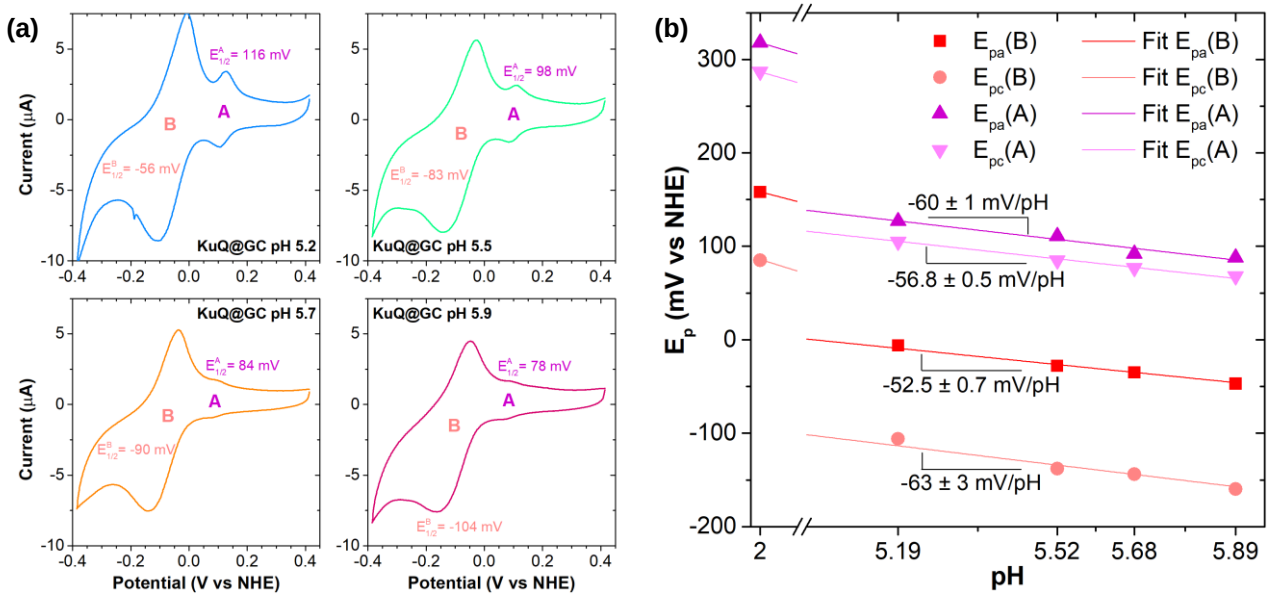

Figure S6. (a) Cyclic voltammograms of KuQ deposited onto glassy carbon (GC, 0.0706 cm^2) electrode in $Na_2SiF_6/NaHCO_3$ buffer at pH varying from 5.2 to 5.9 (CE = Pt, RE = Ag/AgCl 3M NaCl, scan rate = 100 mV/s). The deposition onto GC was achieved by drop-casting 6 µL of 0.23 mM $KuQ(O)_3OH$ solution in THF. **(b)** Plot of the peak potentials (anodic, Epa, and cathodic, Epc) vs the corresponding pH for the two reversible processes, B (orange) related to $KuQ(O)_3O^-$/ $KuQ(O)_3OH^{\bullet -}$ couple and A (purple) related to $KuQ(O)_3OH$/ $KuQ(O)_2(OH)_2^{\bullet}$ couple.

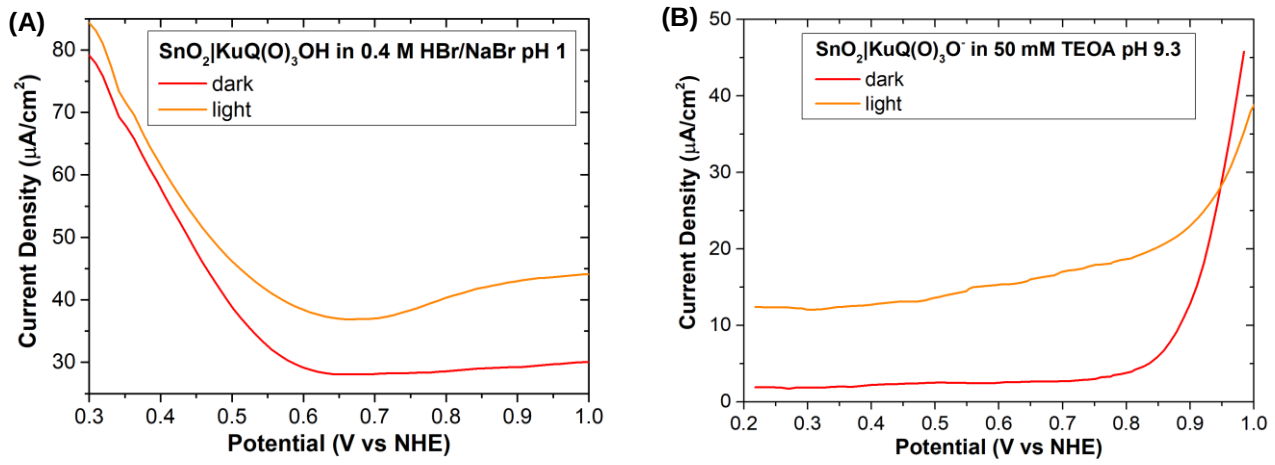

Figure S7. Cyclic voltammetry registered for SnO_2|KuQ photoanodes in (A) 0.1 M HBr, 0.3 M NaBr solution pH = 1 and (B) 0.1 M Na_2SO_4, 50 mM triethanolamine (TEOA) pH = 9.3. CE = Pt, RE = Ag/AgCl 3M NaCl, scan rate = 20 mV/s.

Table S1. Summary of the photoelectrochemical tests of SnO_2|KuQ photoanodes in presence of electron donors in aqueous solution.

pH	Donor	Notes	Onset potential (V vs NHE)	Photocurrent Density, μA/cm² (Potential, V vs NHE)
1	**Br^-**	-	0.5	14 ± 2 (between 0.8-1.0 V)
5.8	**Ascorbate**	-	0.1	400± 20 (at 0.5 V)
9.27	**TEOA**	Detachment of the dye	0.2	13 ± 2 (between 0.2-0.8 V)

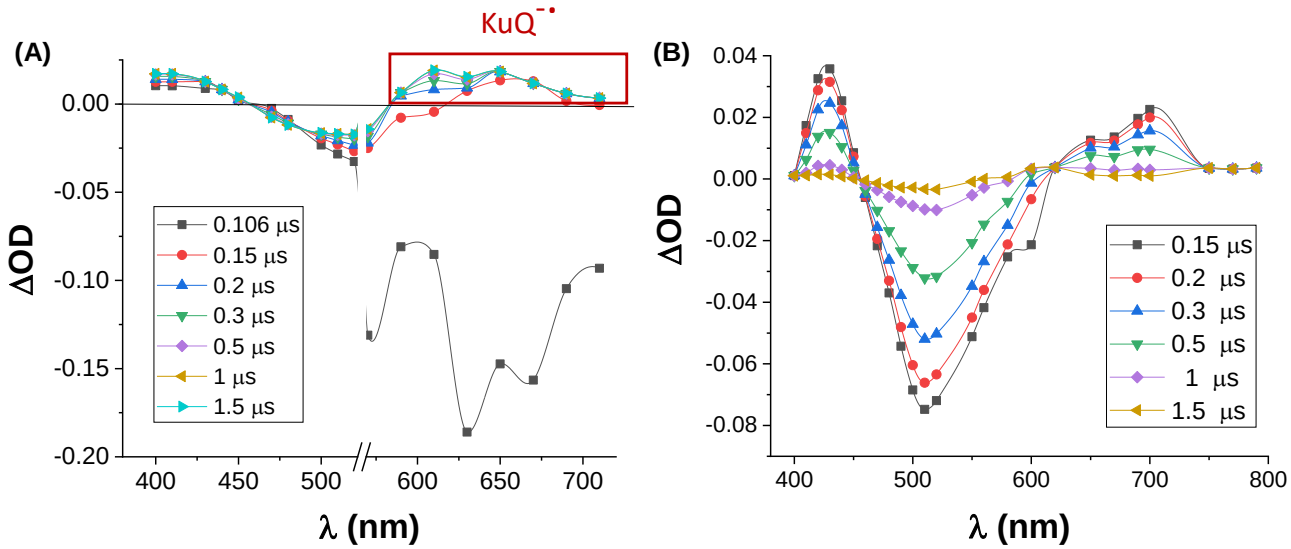

Figure S8. (A) Transient absorption spectra of a $KuQ(O)_3OH$ solution in aerated THF containing 1 M sodium ascorbate aqueous solution (2 drops of 6 M HCl have been also added to restore the violet colour typical of the acid form of the dye) at different delays from the 532 nm ns-laser excitation. The long-living (> 0.5 μs) absorption at λ> 610 nm is attributed to the reduced KuQ dye, which survives far beyond the time window of the experiment (1.5 μs); **(B)** Transient absorption spectra of a $KuQ(O)_3OH$ solution in THF at different delays from the 532 nm ns-laser excitation. The absorptions at λ< 450 nm and at λ> 620 nm are attributed to the population of the lowest triplet state, while the intense signal centered at 510 nm is the ground state bleaching. It is worth noting that, differently than in A, the ground state is almost completely recovered after ca. 1.5 μs.

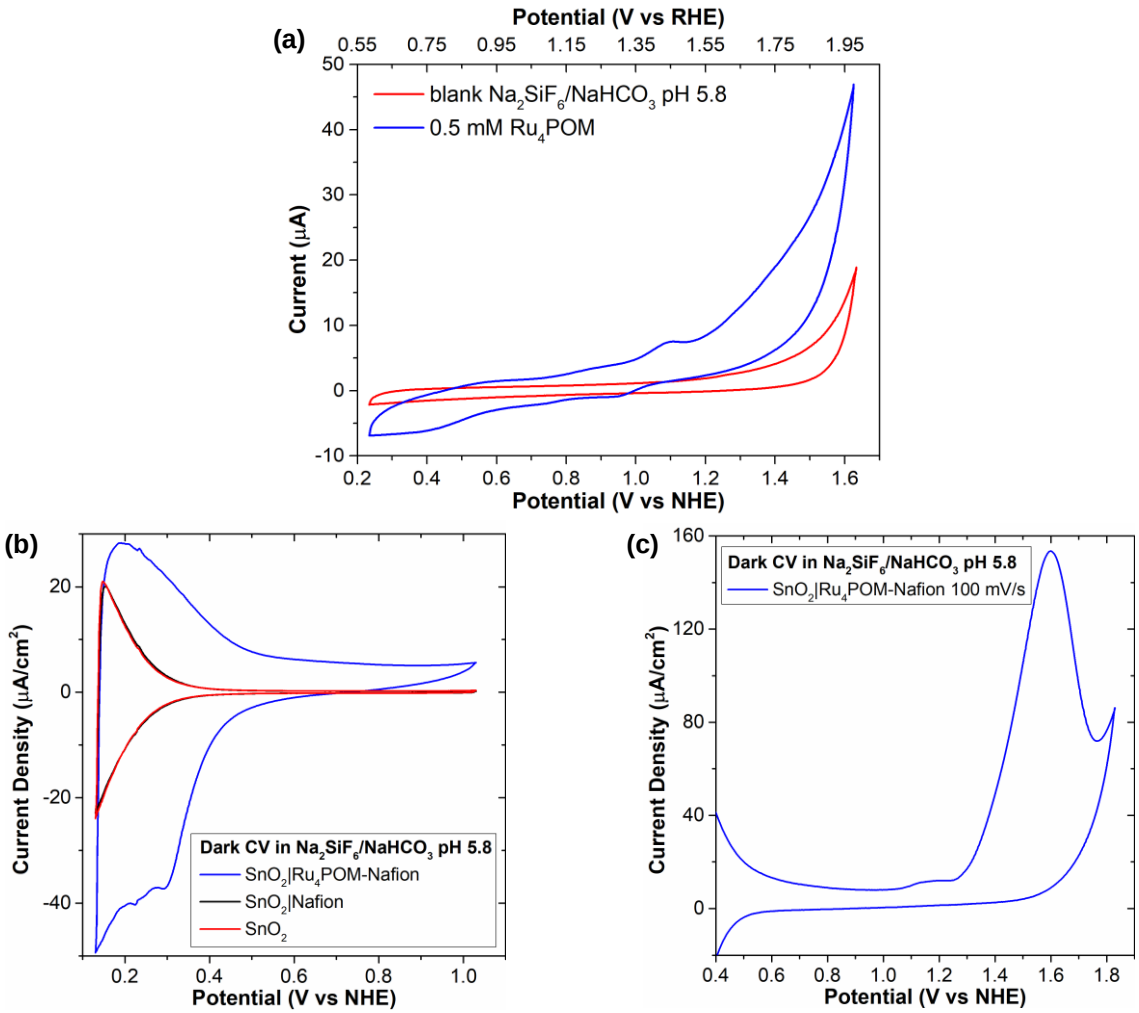

Figure S9. (a) CV of 0.5 mM Ru_4POM catalyst in 0.1 M $Na_2SiF_6/NaHCO_3$ buffer pH 5.8. WE = GC, CE = Pt, RE = Ag/AgCl 3M NaCl, scan rate = 100 mV/s. **(b)** Dark CVs (20 mV/s) of SnO_2 electrodes before and after deposition of Nafion (soaking in 1% Nafion solution) and Ru_4POM-Nafion (soaking in 4 mM Ru_4POM + 1% Nafion), showing that the Nafion matrix does not affect the electrochemical response of SnO_2 electrodes. **(c)** Extended CV for $SnO_2|Ru_4POM$-Nafion, showing the dark catalysis of Ru_4POM: the peak shape, indicating a complete consumption of the catalytic substrate, of the water oxidation catalytic wave (1.3 V-1.7 V) suggests that the Nafion matrix is largely limiting the diffusion of water.

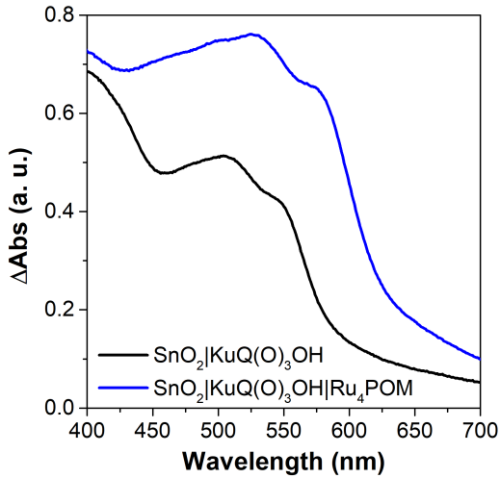

Figure S10. UV-Vis spectra for dye-sensitized electrode $SnO_2|KuQ(O)_3OH$ before (black) and after (blue) functionalization with the Ru_4POM catalyst. SnO_2 contribution has been subtracted.

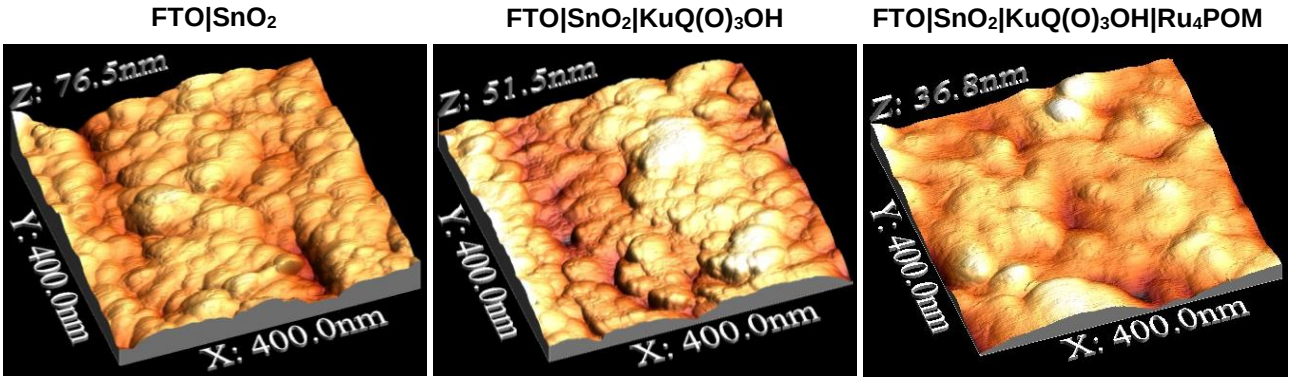

Figure S11. AFM images for the nanostructured SnO_2 electrode (left), dye-sensitized electrode $SnO_2|KuQ(O)_3OH$ electrode (center) and $SnO_2|KuQ(O)_3OH|Ru_4POM$ electrode (right).

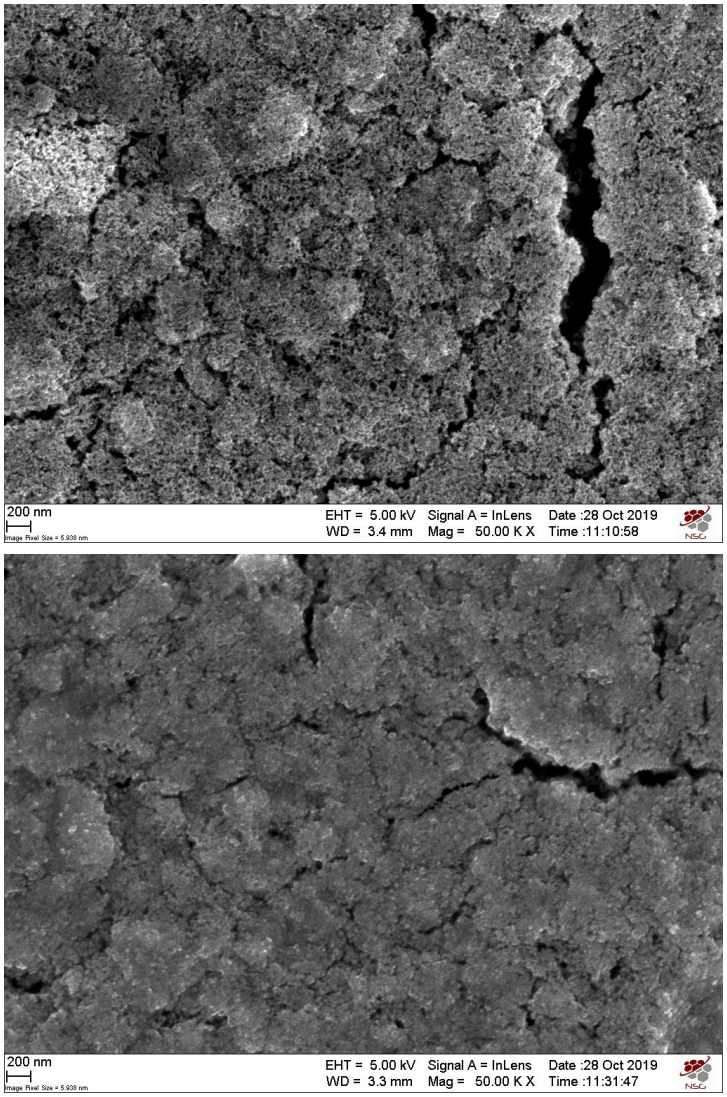

Figure S12. SEM image for $SnO_2|KuQ(O)_3OH$ before (top) and after (bottom) functionalization with the Ru_4POM catalyst by soaking in a 4 mM Ru_4POM solution containing 1% Nafion polymer.

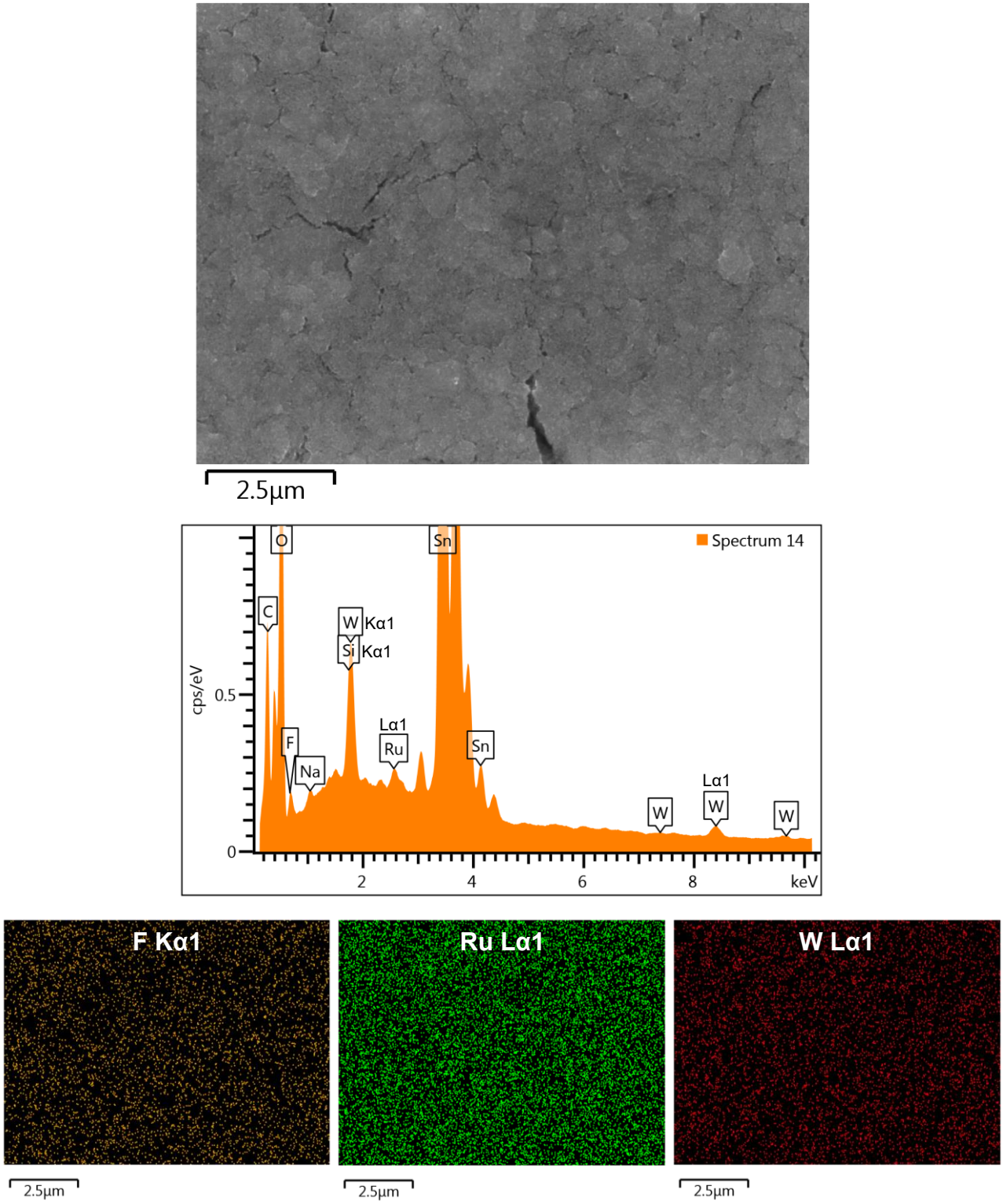

Figure S13. EDX elemental mapping of nanoSnO_2|$KuQ(O)_3OH$|Ru_4POM electrode, showing the homogenous distribution of the Ru_4POM catalyst (see Ru and W map) and of the Nafion matrix (see F map) over the electrode surface. Excitation energy: 20 kV. Ruthenium (4 atoms), tungsten (20 atoms) and silicon (2 atoms) are present in the catalyst molecule, $Na_{10}\{Ru_4(\mu\text{-}O)_4(\mu\text{-}OH)_2[\gamma\text{-}SiW_{10}O_{36}]_2\}$: the Lα1 emission line (ca. 8.4 keV) was selected for the detection of tungsten instead of the stronger Kα1 (ca. 1.7 keV) due to the superimposition of the latter with the Si Kα1; for the same reason, silicon was excluded from EDX mapping. Fluorine was selected for the identification of the Nafion polymer, since the F Kα1 X-rays eventually produced by the FTO substrate are absorbed within less than 1 µm of SnO_2.

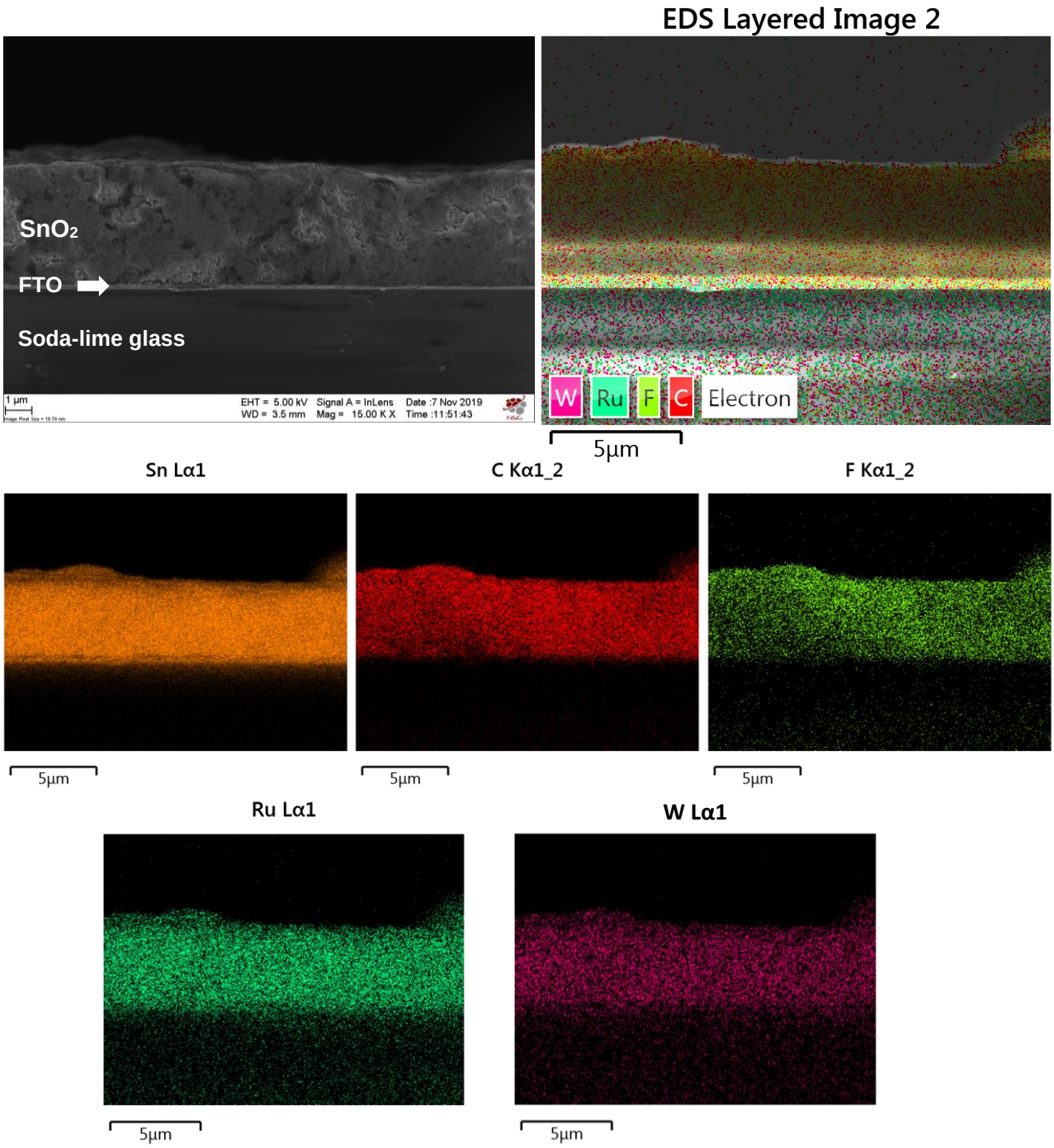

Figure S14. EDX elemental mapping of the cross-section of SnO_2|KuQ$(O)_3$OH|Ru_4POM electrode (excitation energy: 20 kV, acquisition time: 1.5 hours). Top left) SEM image of the cross-section, acquired with an acceleration voltage of 3 kV (InLens detector), and (top right) superimposition of the EDX elemental mapping to the SEM image of the same area, acquired with an acceleration voltage of 20 kV (secondary electron detector). Ruthenium (4 atoms), tungsten (20 atoms) and silicon (2 atoms) are present in the Ru_4POM molecule: the Lα1 emission line was selected for the detection of tungsten instead of the stronger Kα1 due to the superimposition of the latter with the Si Kα1; for the same reason, silicon was excluded from EDX mapping. Fluorine was selected for the identification of the Nafion polymer. The high concentration of carbon in the SnO_2 layer is ascribable both to KuQ molecules and to Nafion polymer. Tin is both present in the nanostructured SnO_2 layer and in the conductive FTO substrate. The contribution of F, Ru and W is found through the whole SnO_2 layer, evidencing the high porosity of the material, which allowed the diffusion of the catalyst/Nafion solution; the small amount of F, Ru and W signals arising from the region beneath the SnO_2 layer is instead ascribable to background noise, due to the low emission intensity of the F Kα1, Ru Lα1 and W Lα1 lines.

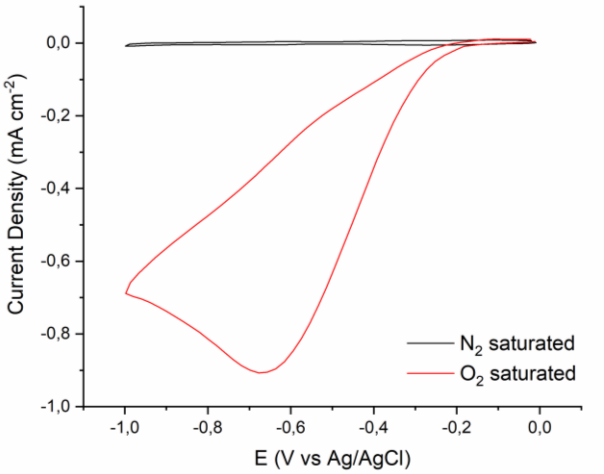

Figure S15. CV recorded for FTO electrode in Na_2SiF_6/$NaHCO_3$ buffer pH 5.8. CV have been carried out in O_2 and N_2 saturated conditions. WE = FTO, CE = Pt, RE = Ag/AgCl 3M NaCl, scan rate = 100 mV/s.

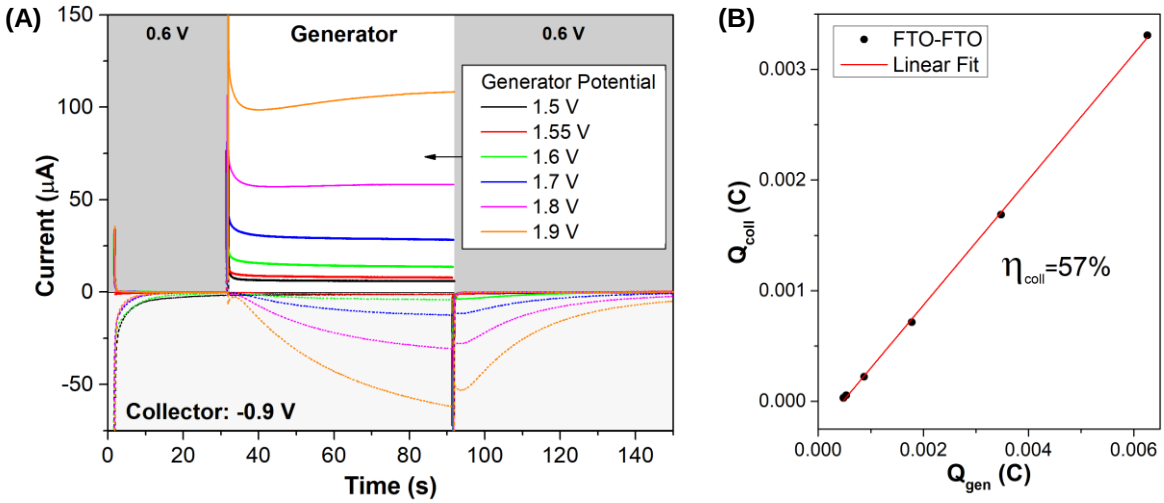

Figure S16. Calibration experiment for the generator-collector method, performed with FTO-FTO sandwich in N_2 purged-Na_2SiF_6/$NaHCO_3$ buffer at pH 5.8. **(A)** Anodic (positive) and cathodic (negative) currents are registered for the same system: the generator was held at a constant potential of 0.6 V vs Ag/AgCl during "off" periods, and at potentials in the range 1.5-1.9 V vs Ag/AgCl during "on" periods; the collector was held at -0.9 V vs Ag/AgCl. (B) Linear relationship between charges associated to anodic (generator) and cathodic (collector) electrodes. Calculation procedure is fully described in the Methods section. A linear, y = ax+b trend is obtained, with a=0.568±0.005 and b=-2.65E-4±1.56E-5.

Table S2. Summary of the results obtained from generator-collector experiments with nanoSnO_2|$KuQ(O)_3OH$|Ru_4POM photoanodes.

Electrode	Measure	Q_{gen} (C)	Q_{coll} (C)	Q_{coll}/Q_{gen}	Faradaic Efficiency (%)
SnO_2|$KuQ(O)_3OH$ (blank)	1st	1.02E-03	2.86E-6	0.003	**<1**
SnO_2|$KuQ(O)_3OH$|Ru_4POM #1	1st	1.63E-03	6.90E-04	0.42	**74**
	2nd	1.26E-3	6.09E-04	0.48	**85**
	3rd	1.27E-4	3.38E-04	0.32	**56**
SnO_2|$KuQ(O)_3OH$|Ru_4POM #2	1st	1.70E-3	6.64E-04	0.39	**69**
	2nd	2E-03	1.15E-03	0.56	**101**
	3rd	9.64E-04	4.05E-04	0.42	**74**

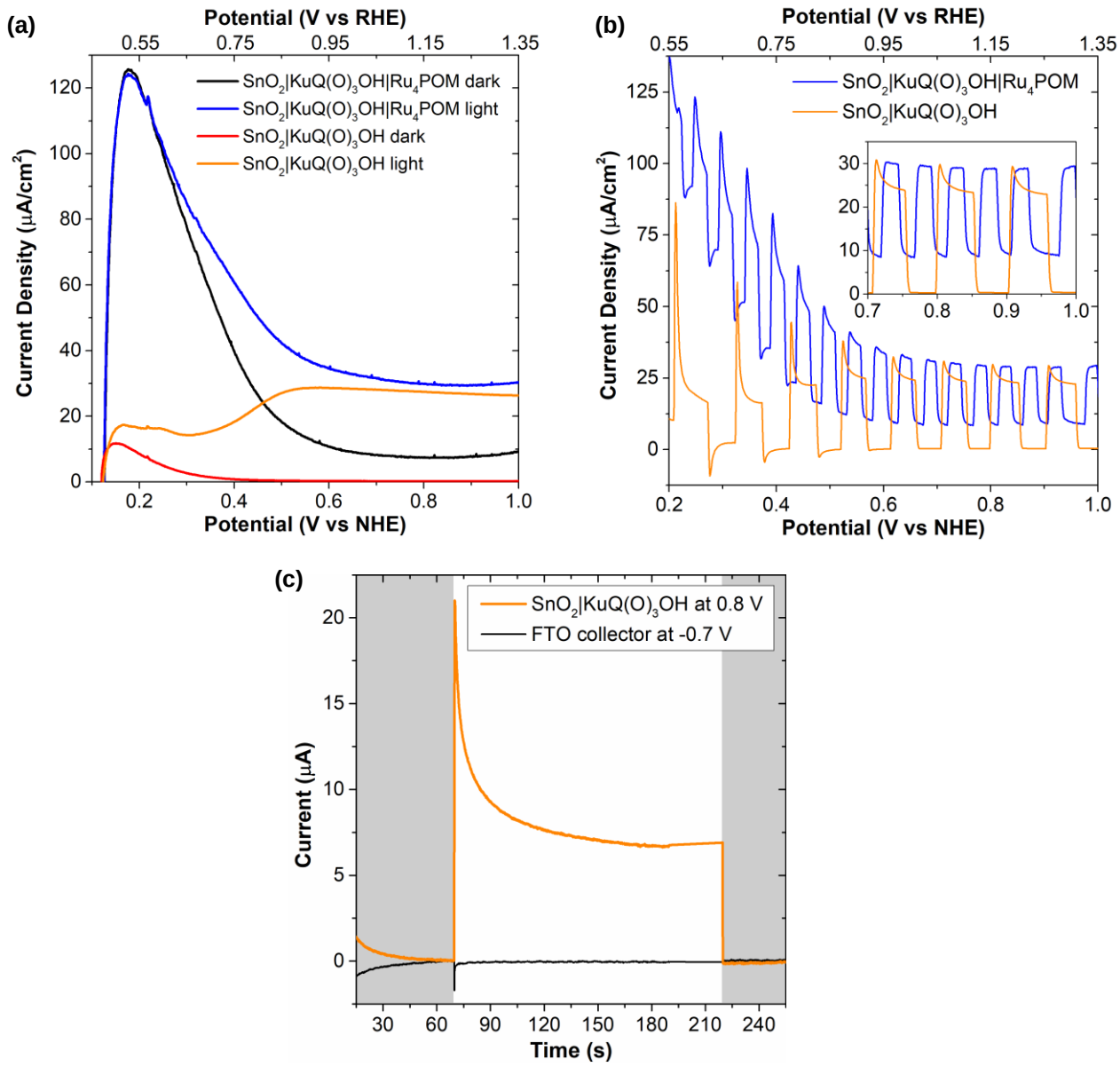

Figure S17. Photoelectrochemical characterization of the photoanodes in 0.1 M Na_2SiF_6/$NaHCO_3$ buffer pH 5.8. **(a, b)** LSV and chopped LSV recorded for SnO_2|$KuQ(O)_3OH$ and SnO_2|$KuQ(O)_3OH$|Ru_4POM-Nafion photoanodes (scan rate = 20 mV/s, CE = Pt, RE = Ag/AgCl 3M NaCl, AM 1.5 G light + 400 nm cut-off filter, back-irradiation). **(c)** Generator-collector experiments for SnO_2|$KuQ(O)_3OH$ photoanodes, showing no evidence of oxygen evolution in the absence of the Ru_4POM catalyst. The currents produced at the generator (anodic) and at the collector (cathodic) are reported: during all experiment, the photoanode was held at a constant potential of 0.8 V vs NHE, while "off" and "on" periods (during which photoanodes are back-illuminated using a white LED lamp and a 400 nm cut-off filter) were alternated; the FTO collector was held at of -0.7 V vs NHE. Electrolytic solution was saturated with N_2 before each measure. The presence of a background cathodic current before the illumination step can be related to the presence of residual traces of oxygen in solution, which are consumed at the collector during the initial dark period.

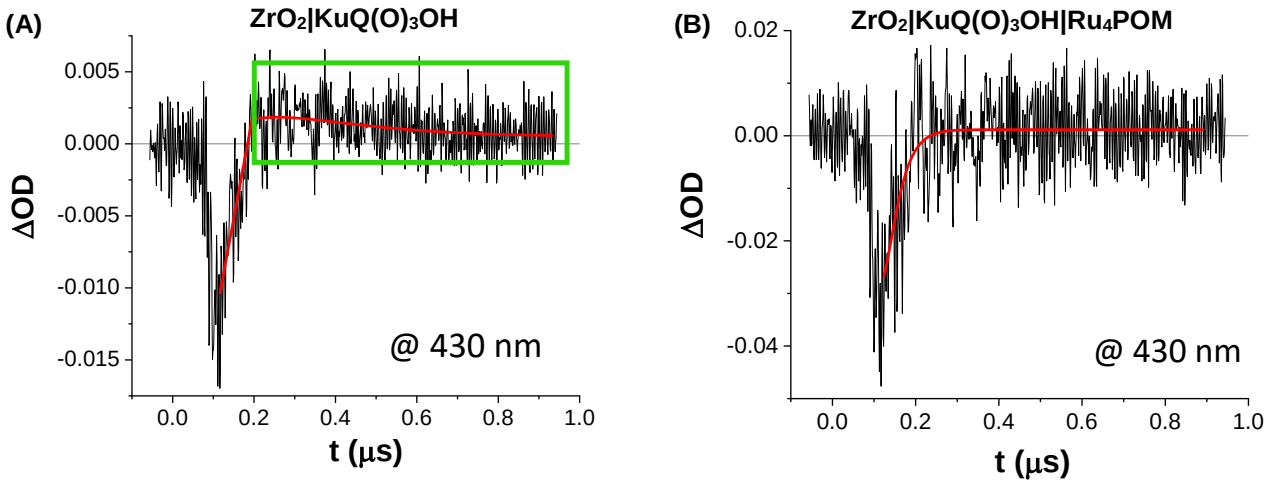

Figure S18. Kinetic evolution of the triplet excited state (tracked at 430 nm) of the $KuQ(O)_3OH$ dye on ZrO_2 in the absence **(A)** or in the presence **(B)** of Ru_4POM, after the 532 nm ns-laser excitation. Traces collected in $Na_2SiF_6/NaHCO_3$ buffer at pH 5.8. The green box of Figure A evidences the presence of the triplet absorption which decays with slow dynamics on the hundreds/thousands nanoseconds timescale, contrasting with the case of $ZrO_2|KuQ_3|Ru_4POM$, where no significant dynamic was detected after the laser pulse. This indicates the presence, in this latter case, of a fast quenching by charge transfer, followed by recombination on a timescale equal or lower than that of the excitation pulse.

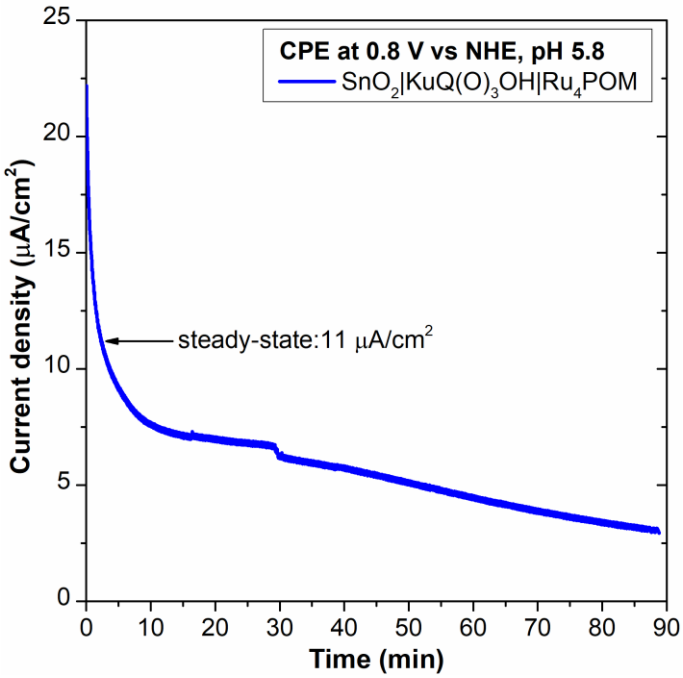

Figure S19. Controlled potential photoelectrolysis with $SnO_2|KuQ(O)_3OH|Ru_4POM$ photoanode at 0.8 V vs NHE in 0.1 M $Na_2SiF_6/NaHCO_3$ buffer pH 5.8. CE = Pt, RE = Ag/AgCl 3M NaCl, AM 1.5 G light + 400 nm cut-off filter, back-irradiation.

Table S3. Summary of the performances reported for the state-of-the-art of water oxidation photoanodes.

System	Onset potential (V vs RHE)	Photocurrent density (μA cm^{-2}) [potential, V vs RHE]	IPCE (%)	APCE (%)	Faradaic Yield (%)
nanoTiO_2 | Ru(bpy)(dpbpy)(mbpy)–$IrO_2 \cdot nH_2O$ [7]	0.2[a]	30 [0.35-0.85]	n.r.	n.r.	20
ITO | PMPDI | CoO_x [8]	0.65[b]	150 [1.65]	0.12	1	80
SnO_2 | PMPDI | CoO_x [9]	0.65[b]	50 [0.81]	0.5-2	n.r	31
WO_3 | PBI | IrO_2 [3]	0.7[c]	70 [0.92]	0.6	0.8	n.r.
WO_3 | {PBI_5Ru_4POM} [10]	0.74[c]	44 [0.91]	0.5	1.3	> 95
FTO | TiO_2 | Bodipy–RuWOC [11]	0.32[d]	60 [0.63][d] 100 [0.55][a]	4	n.r.	44.5
SnO_2 | Porphyrin | Ir-WOC [12]	0.6[e]	40 [1.15]	0.8	n.r.	n.r.
SnO_2 | TiO_2 | Porphyrin | Ir-WOC [13]	0.50[f]	120 [1.24]	0.25	3	> 95
FTO | TiO_2 | SP+Ru-WOC [14]	0.3[d]	60 [0.65]	2	n.r.	64
nanoSnO_2 | $KuQ(O)_3OH$ | Ru_4POM	0.64	10 [0.9]	0.09	0.12	70±15

[(a)] $Na_2SiF_6/NaHCO_3$ pH 5.75; [(b)] 0.1 M pH 7 KPi; [(c)] 0.1 M $NaClO_4$ pH 3; [(d)] NaF 0.1 M pH 7.2; [(e)] 0.1m KNO_3 pH 6; [(f)] 0.1 M HBr pH=1. (n.r.= not reported by authors).

4. References

[1] F. Ronconi, M. P. Santoni, F. Nastasi, G. Bruno, R. Argazzi, S. Berardi, S. Caramori, C. A. Bignozzi, S. Campagna, *Dalt. Trans.* **2016**, *45*, 14109–14123.

[2] M. Bonomo, F. Sabuzi, A. Di Carlo, V. Conte, D. Dini, P. Galloni, *New J. Chem.* **2017**, *41*, 2769–2779.

[3] F. Ronconi, Z. Syrgiannis, A. Bonasera, M. Prato, R. Argazzi, S. Caramori, V. Cristino, C. A. Bignozzi, *J. Am. Chem. Soc.* **2015**, *137*, 4630–4633.

[4] A. Orbelli Biroli, F. Tessore, M. Pizzotti, C. Biaggi, R. Ugo, S. Caramori, A. Aliprandi, C. A. Bignozzi, F. De Angelis, G. Giorgi, et al., *J. Phys. Ch*em. C **2011**, 115, 23170–23182.

[5] (a) S. Hu, M. R. Shaner, J. A. Beardslee, M. Lichterman, B. S. Brunschwig, N. S. Lewis *Science* **2014**, *344*, 1005–1009; (b) R. Matheu, I. A. Moreno-Hernandez, X. Sala, H. B. Gray, B. S. Brunschwig, A. Llobet, N. S. Lewis *J. Am. Chem. Soc.* **2017**, *139*, 11345–11348; (c) S. Grau, S. Berardi, A. Moya, R. Matheu, V. Cristino, J. J. Vilatela, C. A. Bignozzi, S. Caramori, C. Gimbert-Suriñach, A. Llobet, *Sustain. Energy Fuels* **2018**, *2*, 1979–1985.

[6] B. D. Sherman, M. V. Sheridan, C. J. Dares, T. J. Meyer, *Anal. Chem.* **2016**, *88*, 7076–7082.

[7] D. Gust, W. J. Youngblood, Y. Kobayashi, A. L. Moore, T. A. Moore, P. G. Hoertz, E. A. Hernandez-Pagan, T. E. Mallouk, S.-H. A. Lee, *J. Am. Chem. Soc.* **2009**, *131*, 926–927.

[8] J. T. Kirner, J. J. Stracke, B. A. Gregg, R. G. Finke, *ACS Appl. Mater. Interfaces* **2014**, *6*, 13367–13377.

[9] J. T. Kirner, R. G. Finke, *ACS Appl. Mater. Interfaces* **2017**, *9*, 27625–27637.

[10] A. Sartorel, G. La Ganga, N. Marino, N. Demitri, C. A. Bignozzi, F. Rigodanza, S. Caramori, H. Amenitsch, M. Prato, G. A. Volpato, et al., *Nat. Chem.* **2018**, *11*, 146–153.

[11] O. Suryani, Y. Higashino, Y. Mulyana, M. Kaneko, T. Hoshi, J. Y. Mulyana, M. Kaneko, T. Hoshi, K. Shigaki, Y. Kubo, *Chem. Commun.* **2017**, *53*, 6784–6787.

[12] K. L. Materna, J. Jiang, K. P. Regan, C. A. Schmuttenmaer, R. H. Crabtree, G. W. Brudvig, *ChemSusChem* **2017**, *10*, 4526–4534.

[13] A. Orbelli Biroli, F. Tessore, G. Di Carlo, M. Pizzotti, E. Benazzi, F. Gentile, S. Berardi, C. A. Bignozzi, R. Argazzi, M. Natali, A. Sartorel and S. Caramori, *ACS Appl. Mater. Interfaces*, 2019, **11**, 32895–32908.

[14] M. Yamamoto, Y. Nishizawa, P. Chábera, F. Li, T. Pascher, V. Sundström, L. Sun, H. Imahori, *Chem. Commun.* **2016**, *52*, 13702–13705.

5. Cartesian coordinates of optimised geometries

Optimized cartesian coordinates (in Angstroms) for geometry optimization of $KuQ(O)_3OH$ in THF (B3LYP functional 6-31G+(d,p) basis set).

Energy -1413.793137 Hartree
Stoichiometry C25H16O6
Framework group C1[X(C25H16O6)]
Deg. of freedom 135
Full point group C1 NOp 1
Largest Abelian subgroup C1 NOp 1
Largest concise Abelian subgroup C1 NOp 1
Standard orientation:

Center Number	Atomic Number	Atomic Type	Coordinates (Angstroms) X	Y	Z
1	6	0	0.144263	-1.407502	-0.038959
2	6	0	0.995371	-0.295526	-0.209932
3	6	0	-1.203612	-0.922167	-0.031749
4	6	0	2.451163	-0.460402	-0.275328
5	6	0	0.625130	-2.759556	0.088363
6	6	0	-1.142306	0.499099	-0.197752
7	6	0	2.964697	-1.868594	-0.143905
8	8	0	3.234469	0.480548	-0.428947
9	6	0	0.206406	0.895571	-0.311228
10	6	0	2.089889	-2.967326	0.032634
11	8	0	-0.154024	-3.739011	0.240419
12	6	0	4.342981	-2.093654	-0.194735
13	6	0	2.611154	-4.261972	0.154347
14	6	0	4.855140	-3.387924	-0.072766
15	1	0	5.003790	-1.244343	-0.329847
16	6	0	3.989632	-4.472498	0.102126
17	1	0	1.927191	-5.092520	0.289335
18	1	0	5.927875	-3.549354	-0.113702
19	1	0	4.387270	-5.477948	0.197333
20	6	0	0.705506	2.299653	-0.487854
21	1	0	0.012431	2.835413	-1.144005
22	1	0	1.691840	2.275314	-0.955650
23	6	0	-3.652908	0.550971	-0.126864
24	6	0	-3.678962	-0.857094	0.039707
25	1	0	-4.824925	2.330070	-0.303982
26	6	0	-4.857871	1.253543	-0.177266
27	6	0	-4.908218	-1.524240	0.152363
28	6	0	-6.103519	-0.806527	0.099063
29	6	0	-6.078711	0.581486	-0.066450
30	1	0	-4.918513	-2.600482	0.280477
31	1	0	-7.050596	-1.329197	0.186240
32	1	0	-7.008045	1.140837	-0.108823
33	6	0	-2.422068	-1.609442	0.089662
34	6	0	-2.357368	1.307889	-0.243024
35	8	0	-2.358672	2.538389	-0.364321
36	8	0	-2.501716	-2.903190	0.242346
37	1	0	-1.547786	-3.330656	0.255748
38	6	0	0.790296	3.065988	0.854526
39	1	0	1.532854	2.592386	1.504778

40	1	0	-0.178007	3.006897	1.360497
41	6	0	1.135899	4.549161	0.670336
42	1	0	1.001177	5.078920	1.623313
43	1	0	0.463341	5.028764	-0.047025
44	6	0	2.567626	4.809702	0.259762
45	8	0	3.533520	4.144403	0.585708
46	8	0	2.687532	5.924345	-0.500020
47	1	0	3.633566	6.060205	-0.686632

Rotational constants (GHZ): 0.1518312 0.1241975
0.0692613

Optimized cartesian coordinates (in Angstroms) for geometry optimization of $KuQ(O)_3O^-$ in THF (B3LYP functional 6-31G+(d,p) basis set).

Energy -1413.324489 Hartree
Stoichiometry C25H15O6(1-)
Framework group C1[X(C25H15O6)]
Deg. of freedom 132
Full point group C1 NOp 1
Largest Abelian subgroup C1 NOp 1
Largest concise Abelian subgroup C1 NOp 1
Standard orientation:

Center Number	Atomic Number	Atomic Type	Coordinates (Angstroms) X	Y	Z
1	6	0	0.078468	-1.448584	0.016287
2	6	0	0.923405	-0.294136	-0.132155
3	6	0	-1.268844	-0.987826	0.017634
4	6	0	2.373912	-0.368542	-0.180263
5	6	0	0.650376	-2.788626	0.119855
6	6	0	-1.227016	0.443462	-0.127666
7	6	0	2.971542	-1.742671	-0.122880
8	8	0	3.117840	0.624727	-0.262379
9	6	0	0.120994	0.869391	-0.226267
10	6	0	2.155031	-2.882633	0.019112
11	8	0	0.003637	-3.831046	0.279040
12	6	0	4.362862	-1.889662	-0.204742
13	6	0	2.751612	-4.149820	0.073795
14	6	0	4.946310	-3.155267	-0.152709
15	1	0	4.971795	-0.997996	-0.308873
16	6	0	4.136864	-4.289313	-0.013198
17	1	0	2.110433	-5.017579	0.184885
18	1	0	6.025415	-3.259349	-0.219565
19	1	0	4.585329	-5.277777	0.028381
20	6	0	0.607604	2.280028	-0.409529
21	1	0	-0.138013	2.846184	-0.974236
22	1	0	1.542227	2.259228	-0.975306
23	6	0	-3.731917	0.556981	-0.112032
24	6	0	-3.787784	-0.844746	0.025392
25	1	0	-4.851572	2.373657	-0.294449
26	6	0	-4.920003	1.296091	-0.190573
27	6	0	-5.037274	-1.477141	0.082432
28	6	0	-6.216090	-0.735606	0.000635

29	6	0	-6.158104	0.656604	-0.137156
30	1	0	-5.064167	-2.555926	0.191147
31	1	0	-7.177307	-1.239669	0.044255
32	1	0	-7.073359	1.237956	-0.201610
33	6	0	-2.542886	-1.697341	0.114878
34	6	0	-2.416862	1.275210	-0.167112
35	8	0	-2.395268	2.517379	-0.238261
36	8	0	-2.675003	-2.919792	0.256873
37	6	0	0.848662	3.001239	0.933727
38	1	0	1.590856	2.451841	1.522594
39	1	0	-0.083436	3.012805	1.507866
40	6	0	1.313896	4.465471	0.765087
41	1	0	1.341960	4.947533	1.747532
42	1	0	0.614316	5.014636	0.129091
43	6	0	2.708171	4.561872	0.193411
44	8	0	3.732365	4.291143	0.796515
45	8	0	2.728022	4.979233	-1.094880
46	1	0	3.655200	4.984688	-1.392738

Rotational constants (GHZ): 0.1642557 0.1187388
0.0702506